



**HAL**  
open science

## 3D visualization of PEMFC electrode structures using FIB tomography

Susanne Zils, Melanie Timpel, Tobias Arlt, André Wolz, Ingo Manke,  
Christina Roth

► **To cite this version:**

Susanne Zils, Melanie Timpel, Tobias Arlt, André Wolz, Ingo Manke, et al.. 3D visualization of PEMFC electrode structures using FIB tomography. *Fuel Cells*, 2010, 10 (6), pp.966. 10.1002/fuce.201000133 . hal-00591286

**HAL Id: hal-00591286**

**<https://hal.science/hal-00591286>**

Submitted on 9 May 2011

**HAL** is a multi-disciplinary open access archive for the deposit and dissemination of scientific research documents, whether they are published or not. The documents may come from teaching and research institutions in France or abroad, or from public or private research centers.

L'archive ouverte pluridisciplinaire **HAL**, est destinée au dépôt et à la diffusion de documents scientifiques de niveau recherche, publiés ou non, émanant des établissements d'enseignement et de recherche français ou étrangers, des laboratoires publics ou privés.



### 3D visualization of PEMFC electrode structures using FIB tomography

Journal:	<i>Fuel Cells</i>
Manuscript ID:	fuce.201000133.R1
Wiley - Manuscript type:	Original Research Paper
Date Submitted by the Author:	22-Sep-2010
Complete List of Authors:	Zils, Susanne; Technische Universität Darmstadt, Department of Materials Science Timpel, Melanie; Helmholtz Centre Berlin for Materials and Energy, Department of Functional Materials Arlt, Tobias; Helmholtz Centre Berlin for Materials and Energy, Department of Functional Materials Wolz, André; Technische Universität Darmstadt, Department of Materials Science; CRP Henri Tudor, Department of Advanced Materials and Structures Manke, Ingo; Helmholtz Centre Berlin for Materials and Energy, Department of Functional Materials Roth, Christina; Technische Universität Darmstadt, Department of Materials Science
Keywords:	Polymer Electrolyte Membrane Fuel Cell, Focused Ion Beam, Tomography, Water Management, Electrode structure

SCHOLARONE™  
Manuscripts

1  
2  
3 September 22, 2010  
4  
5

6 **Dear Mrs Bele:**  
7

8  
9 We thank you for your kind letter and for sending the referees' responses. We very much  
10 appreciate the comments of the referees, which will help us to further improve our paper and  
11 make it accessible also to readers with less background in materials characterization. Please  
12 find enclosed our reply to the referees' remarks and suggestions along with the revised paper.  
13 Changes to the paper's text body are marked in red in the attached document. We would like  
14 to mention that the reference introduced by reviewer #1 is an abstract for a symposium which  
15 took place after we submitted this paper. We thank the referees for their thorough review and  
16 look forward to your final decision.  
17  
18  
19

20  
21 Best regards,  
22 Susanne Zils  
23  
24

---

25  
26  
27  
28 Response reviewer #1:  
29

30  
31 *Comments:*

32 *The manuscript is very promising but it is eye-catching that your focus is the experimental*  
33 *work. Please extend the sections regarding the single cell tests - they should be described in a*  
34 *manner that they are reproducible. The major outcome is the comparison of the degradation*  
35 *of the 2 MEAs, therefore I would expect a diagram of the degradation curves.*  
36

37 We agree with the referee; the focus of our work definitely is on the development and first  
38 real application of the FIB technique towards fuel cell components. This technique has not  
39 been used at the membrane-electrode interface before in order to compare different MEA  
40 preparation techniques. The main emphasis of this paper is on how to prepare the samples and  
41 how to do the complex measurements in order to obtain meaningful results. So our main aim  
42 was to show the promising perspectives this new technique has to offer to the fuel cell  
43 community, not just complementing Hg porosimetry and SEM analysis, but indeed providing  
44 3D information on the electrode structure in an unprecedented way.  
45  
46  
47  
48  
49

50 In contrast to the referee's comment, this paper was not intended to study degradation  
51 phenomena in greater detail. This is something that will have to be done in future work and is  
52 just an outlook. Of course, this is the real potential of the FIB technique – one could even  
53 think about site-selective degradation studies and recommendations on how to best prepare an  
54 electrode. But these studies will take much more time.  
55  
56  
57  
58  
59  
60

### Formalism

- *Formatting: In the 2nd and 3rd line of the abstract, two dashes were used with different symbols (“–“ and “-“).*
- *Numbering of the equation (1) in section 3.3 (formatting)*

Formatting has been corrected.

### Minor revisions

**Tortuosity.** *In section 1, Ostadi [17] is referenced who calculated the tortuosity from lattice Boltzmann simulations. In section 3.3 the tortuosity is introduced as a geometric tortuosity by eq. (1). It should at least be noticed that the tortuosity calculated by Ostadi [17] is based on flow simulations which might be different from the geometric tortuosity in certain situations. Optional: Is it possible to compare the two definitions with the determination of the tortuosity by Hg porosimetry mentioned in the introduction / [11]?*

We agree with the referee, it should definitely be noted if two different tortuosity calculation principles are referred to in the text. This notion has been added to the corresponding section. The tortuosities of the cited paper and the calculated geometric tortuosities should not be compared - but not only because of the two different calculation principles. Ostadi et al. [18] calculated the tortuosities for MPLs which consist of carbon black and Teflon<sup>®</sup>. Our work, however, concentrates on the structure of electrodes which consist of carbon supported Pt without Teflon<sup>®</sup>. (p. 4, lines 41-42)

**Section 3.2.** *Last sentence: “According to the more homogeneous... increased amount of TBP” → “... increased amount of TBP ...”.*

The last sentence in section 3.2 has been rewritten with respect to the referee’s suggestion (p. 4, lines 18-21)

**Section 3.3.** *Please specify more details on the methods of obtaining structural parameters.*

Details on the methods for obtaining structural parameters have been added to the table caption of table 1, in order to achieve a better comparability. (p. 6, lines 14-17)

**Section 4.** *“...we were the first to apply the FIB nanotomography technique to MEAs for PEMFCs.” Please compare [R-1].*

The reviewer is absolutely right. This reference is missing and is now cited in the conclusion (section 4). (p. 5, lines 11-13)

### Major revisions

#### Section 1.

- *Introduction, 2nd paragraph: “As the gases and the water use the same pathways through the GDL and the electrode [4]”: This is not said in this simplified manner by Zhang et al [4], they suggest in their conclusion (for example): “the catalyst layer (CL) should have an optimal distribution of hydrophilic and hydrophobic pores...” However, the conclusion (“porosity and pore size distribution play a major role”) is correct – maybe from a different reason.*

1  
2  
3 The corresponding section has been improved by citing Zhang et al. [4] more closely. In our  
4 work we are concentrating on the experimental work of applying FIB nanotomography to  
5 PEMFC electrodes. Therefore we focused on the parameters obtainable by this method, such  
6 as porosity, pore sizes and tortuosity. (p. 1, lines 49-52)  
7  
8  
9

### 10 **Section 2.3.**

- 11 • *Size of the MEA?*
- 12 • *“Polarization curves .... after several days ...” –how much days?*

13 The experimental part for the single cell tests has been extended by the size of the MEA, the  
14 cell equipment used and the conditioning parameters. (p. 3, lines 38 and 41)  
15  
16  
17

### 18 **Section 3.2.**

- 19 • *last sentence: “According to the more homogeneous ... increased amount of TPB ...*  
20 *increased performance... [28]”. It is not clear, what was concluded from [28] and what was*  
21 *concluded from somewhere else. Was the mathematical model from [28] applied to the MEA*  
22 *structure (AB and/or ML)? If yes: how was is done?*

23 We agree with the reviewer, it was not clear what was concluded from O’Hayre et al. [28].  
24 Therefore we pointed out the main proposition of their work and adjusted our conclusion  
25 concerning the relation between the TPB width and the structure characteristics of our ML  
26 MEA. (p. 4, lines 18-21)  
27  
28  
29  
30  
31

### 32 **Section 3.3.**

- 33 • *last sentence: “A direct connection ... is favored for the removal of liquid water...”: is this*  
34 *in agreement with Zhang et al [4] who investigated on hydrophobicity and pore sizes?*  
35 *(similar in section 3.4).*

36 As already discussed in the major revision part for section 1, different hydrophobicities were  
37 not the objective of this work. The proposition that “A direct connection enhances the gas  
38 transport within the electrodes and is favored for the removal of liquid water out of the cell” is  
39 an assumption based on our experience, rather than deduced from literature.  
40  
41  
42  
43

### 44 **Section 3.4.**

- 45 • *Please specify the testing conditions in detail (e. g. size of the fuel cell; are the operating*  
46 *conditions the same as in section 2.3?,...)*

47 Section 2.3 is the experimental part to section 3.4. Hence, the testing conditions are explained  
48 in section 2.3. This has been pointed out in section 3.4. (p. 4, line 54)  
49  
50  
51

- 52 • *again: how much are “several days”?*
- 53 • *Please define “mean maximum power density”*

54 The definition of the parameter mean maximum power density as well as the number of  
55 measurement days have been added. (p. 4, line 60)  
56  
57  
58

- 59 • *A figure of the decrease of the mean maximum power density of both fuel cells would be*  
60 *fine (plot over time). This is the central result of the comparison of the two MEAs.*

1  
2  
3 We do not agree that the degradation of the MEAs is the central result of this work. This  
4 paper is giving an outlook on the possibilities of structural characterization by FIB  
5 nanotomography. We do agree that in future works, the degradation of MEAs should be in the  
6 focus of investigation. (p. 5, line 4)  
7  
8  
9

10 ● *Minor revision, for interest: When the maximum power density decreases – does the current*  
11 *density change where the maximum power density occurs?*

12 We find that a decrease in the current density can be observed when the maximum power  
13 density decreases. This effect is stronger for the AB MEA compared to the ML MEA.  
14  
15  
16

#### 17 **Section 4.**

18 *In the conclusion, current density is a criterion (“... which claim a higher current*  
19 *Density...”)* but in the preceding section there was always argued with the maximum power  
20 *density. A bridge between the two argumentations is missing.*

21 In section 3.2 we discussed that the electrode thickness of the ML MEA is higher than the  
22 electrode thickness of the AB MEA. The cited works of Boyer et al. [26] and Wang et al. [27]  
23 proposed that a thinner electrode will result in less mass transport limitations and therefore in  
24 higher current densities. Higher power densities are usually obtained for MEAs who reach  
25 higher current densities. Hence, section 4 tries to give an outlook on future work on structure  
26 and thickness optimized ML MEA electrodes. (p. 5, lines 18-20)  
27  
28  
29  
30  
31

#### 32 **References**

33 **[R-1]** B. Schwanitz, H. Schulenburg, J. Krbanjevic, M. Stampanoni, A. Wokaun, G.G. Scherer,  
34 “Rapid Aging of Polymer Electrolyte Fuel Cell Electrodes 3D Morphological Study by High-  
35 Resolution X-ray Tomography and FIB/SEM Serial Sectioning”, *TRANSPORT IN POROUS*  
36 *MATERIALS*, 19. - 20.8.2010, PSI in Villigen (Switzerland), abstract book available at  
37 [http://nm.web.psi.ch/transpore2010/Abstract\\_Book\\_Transpore2010.pdf](http://nm.web.psi.ch/transpore2010/Abstract_Book_Transpore2010.pdf)  
38  
39

40 This reference has been added to the list of references, accordingly. (p. 6, lines 2-3)  
41  
42  
43  
44  
45  
46  
47  
48  
49  
50  
51  
52  
53  
54  
55  
56  
57  
58  
59  
60

Response reviewer #2:

*The paper describes using sophisticated FIB nanotomography method to reveal the internal structure of two differently fabricated MEAs of PEMFC. Porosity, pore size distribution and tortuosity of MEAs have been obtained through the real 3D images and compared. In addition, single cell tests have been performed and discussed.*

*In my view, the paper shows an elegant work and worth of publication in Fuel Cell after some minor revisions as follows:*

1) *page 2: lines 22-30, in focused ion beam tomography description, an important reference is missed:*

*Kubis A. J., Shiflet G. J., Dunn D. N., Hull R, Metall Mater Trans A, v35 (7), 1935-1943, 2004.*

Above reference has been included in the text (p. 2, line 22) as reference number [15].

2) *Please correct typo errors i.e. page 2 line 46: "herein after" should be "hereinafter" and page 3 line 25: heating rate of "5 C min-1" should be "5 °C min-1 "*

Typos have been corrected accordingly.

3) *Authors need to clarify the source of uncertainties in table 1. for example, if voxel sizes as mentioned on page 3 lines 14-15 are 9.3X9.3X12.5 nm and 14.8X14.8X14.5 nm then how the uncertainty of average pore diameter on page 4 line 5 is  $\pm 5$  nm? is this uncertainty caused by small threshold variations or something else?*

The uncertainties were calculated by standard deviation and updated in the paper to  $\pm 143$  nm for the AB MEA and  $\pm 76$  nm for the ML MEA. The software package VGStudioMax 2.0 was not able to calculate pore sizes. Therefore, pore sizes have been measured with the semi-automatic software LINCE using the SE micrographs from FIB tomography. (standard deviation included in paper, p. 3, lines 28-30)

4) *It is not quite clear that how many slices have been used for reconstructions. On page 3 section 2.2, the number of milled slices, the time required for milling and the image processing/calculation duration should be declared.*

Details on the process have been included. (included in paper, p. 3, lines 9-11)

5) *In focused ion beam tomography usually a protective layer (typically Pt) is deposited on the surface prior to the milling in order to reduce the redeposit ion effect. In the experiment, have you used such a protective layer? if yes what type of material?. Also has any reference mark (known as fiducial mark) been used to align the images?*

The reviewer is absolutely right, a Pt protective layer with a thickness of 700 nm was deposited on the sample surface to minimize the redeposition of milled material. A fiducial mark has been set, but the automatic drift correction could not be used due to FIB software issues. However, for drift correction a post-processing procedure was applied using the software ImageJ with the Stackreg Plugin and a second marker. (included in paper; p. 3, lines 3-4, line 12)

1  
2  
3  
4  
5 6) *Although, authors refer to Otsu threshold algorithm [24], a short description on how they*  
6 *apply the method on the images will improve the paper. I think threshold variation plays a key*  
7 *role in the uncertainties reported in table 1.*  
8

9 We agree with the referee, threshold variations are crucial factors that have to be considered  
10 as uncertainties for the parameters listed in table 1. We described how the Otsu threshold  
11 algorithm was applied to the images. (included in paper, p. 3, lines 13-18)  
12

13 Furthermore, we extended table 1 by the mean pore sizes determined from the  
14 ultramicrotomic thin-sections which show good agreement with the mean pore sizes  
15 determined by FIB tomography. This shows that the chosen threshold leads to results with  
16 high accuracy.  
17  
18

19  
20 7) *Parameters need to be clearly defined especially when different methods are available to*  
21 *represent them. There are at least two assumptions to represent the pores and pore size*  
22 *distribution. For instance, in mercury porosimetry pores are considered as cylinders while in*  
23 *sphere fitting method (normally used by tomography techniques) pores are assumed to be*  
24 *connected spheres in the pore space. Please mention what type of assumption has been*  
25 *employed. This probably helps other researchers to compare their results with yours.*  
26  
27

28 In our work, pores are considered by the connected spheres model. This has been added in the  
29 text on p. 3, line 24.  
30  
31

32 8) *The tortuosity direction is not clear in the manuscript. It seems that authors have*  
33 *calculated the 1D tortuosity in the main flow direction. In equation (1) the "(1)" is mixed with*  
34 *the tortuosity formula.*  
35

36 For clarification, the main flow direction, in which the 1D tortuosity was calculated, has been  
37 inserted in the text (p. 4, line 47).  
38  
39

40 9) *In figure 1, the 1.6 um long side seems to be the direction of milling and the 2.4 um side is*  
41 *along with the direction of flow. Please make it clear. As mentioned above, this will clarify in*  
42 *which direction the tortuosity has been obtained.*  
43

44 In order to make the milling direction more clear, coordinates have been implemented in the  
45 figure and the milling direction (z-direction) has been noted in the text (p. 3, line 47).  
46  
47  
48  
49  
50  
51  
52  
53  
54  
55  
56  
57  
58  
59  
60

# 3D visualization of PEMFC electrode structures using FIB nanotomography

Susanne Zils<sup>1\*</sup>, Melanie Timpel<sup>2</sup>, Tobias Arlt<sup>2</sup>, André Wolz<sup>1,3</sup>, Ingo Manke<sup>2</sup>, Christina Roth<sup>1</sup>

<sup>1</sup> Department of Materials Science, Technische Universität Darmstadt, Petersenstr. 23, 64287 Darmstadt, Germany

<sup>2</sup> Department of Functional Materials, Helmholtz Centre Berlin for Materials and Energy, Hahn-Meitner-Platz 1, 14109 Berlin, Germany

<sup>3</sup> Department of Advanced Materials and Structures, CRP Henri Tudor, 66 rue de Luxembourg, 4002 Esch-sur-Alzette, Luxembourg

[\*] Corresponding author, [su\\_zils@energy.tu-darmstadt.de](mailto:su_zils@energy.tu-darmstadt.de)

## Abstract

It is well known that the electrode structure of a PEMFC has a huge influence on the water management and thereby on the cell performance. In this work, two MEAs - one prepared by an airbrushing technique and the other by a novel fast spray coating technique (multilayered MEA) - were analyzed with respect to porosity, pore size distribution, tortuosity and their electrochemical performance. FIB nanotomography with following 3D reconstruction, SEM investigation on ultramicrotomic thin-sections, and single cell tests were performed on these MEAs. The results show a higher porosity and lower pore size for the multilayered MEA. The multilayered MEA reaches a Pt utilization of 1962 mW mg<sup>-1</sup> and a peak power density of 210 mW cm<sup>-2</sup>, whereas the airbrushed MEA only provides a Pt utilization of 879 mW mg<sup>-1</sup> and a peak power density of 218 mW cm<sup>-2</sup>. The Pt utilization calculations showed in combination with the structural characterizations that a homogeneous pore structure and Pt distribution provide an advantage with regard to performance and efficiency of the PEMFC. Furthermore, the multilayered MEA may offer an advantage over the airbrushed MEA in its long term stability, which was **observed in preliminary tests**.

Keywords: Focused Ion Beam, tomography, polymer electrolyte membrane fuel cell, water management, electrode structure

## 1 Introduction

Membrane electrode assemblies (MEA) for polymer electrolyte membrane fuel cells (PEMFC) consist of a proton conducting membrane and two electron- and proton conducting electrodes. Beyond the electron- and proton conducting part, the electrodes have to provide for the reactant supply of the MEA. This results in a complex structure of electron and proton conducting parts as well as pores for the gas supply. The so-called triple phase boundary, (TPB) where the electrochemical reactions in the PEMFC take place, can be improved by optimizing the ratio between electron conducting parts (e.g. carbon supported Pt), proton conducting parts (e.g. Nafion<sup>®</sup> ionomer), and gas phase (pores in the electrodes). This will lead to an increased PEMFC performance.

Porosity, pore size distribution, agglomeration of both the catalyst and the proton conducting polymer Nafion<sup>®</sup> as well as the electrode thickness are parameters, which are all most crucial towards the water management in the electrodes, and therefore for the performance of the PEMFC. Water formation and its transport in the fuel cell is an extensive research area. Previous studies showed that well hydrated Nafion<sup>®</sup> membranes maintain a high proton conductivity. This is due to the Grotthuss mechanism, which claims that protons diffuse through the membrane via the hydrogen bond network of water molecules [1, 2]. The water required for this mechanism is supplied by both the humidification of the anode gas and the water produced at the cathode side of the fuel cell. The water molecules of the humidified anode gas are transported from the gas diffusion layer (GDL) through the electrode and the membrane to the cathode side due to the electro-osmotic drag in the MEA. This movement is compensated by the back diffusion of water due to the concentration gradient between anode and cathode [3]. **Zhang et al. [4] claim that reactants and products use the same pathways through the hydrophobic pores of the electrodes, whereas hydrophilic pores only facilitate the liquid water removal. They also suggest that a reduction of the pore diameter and an increase of the hydrophobicity will decrease flooding effects. Hence, porosity and pore size distribution of the electrode play a major role in the fuel cell's water management [4]. In order to improve the porosity and pore size distribution, it is important to analyze and optimize the electrode's structure.**

Over the last years, several analyzing techniques have been used to reveal the electrode structure of PEMFC MEAs. Most of the previous studies were based on electron microscopy as the method of choice. Rolison et al [5] analyzed the advantages of catalytic nanoarchitectures by scanning electron microscopy (SEM) and transmission electron microscopy (TEM). Both methods are fully capable of displaying the 2D structure of the samples, which are investigated. But a 2D image only reflects an extremely small volume of the sample and should therefore be interpreted by keeping this fact in mind.

The most prominent disadvantage of the standard electron microscopy investigations shows in the volume, which is being investigated. Sample preparation techniques such as breaking the MEA under liquid nitrogen [6] or cutting small slices off the MEA either by a scalpel [7] or a razor blade [8] provide only a small volume fraction of the MEA. Furthermore, only the surface of this volume fraction can be investigated. Therefore, no 3D information is obtained by electron microscopy in combination with the standard preparation techniques. Beyond that, different other obstacles occur while preparing samples for electron microscopy investigations. Cutting slices off the MEA may cause damage of the real pore structure or smearing of the membrane [7]. Breaking the MEA under liquid nitrogen may lead to falsely interpreted inhomogeneities in the electrode structure due to agglomerates, which might be pulled out of the surface during the sample preparation [6]. In order to minimize these artifacts, an advanced sample preparation method has been developed recently by Blom et al. [9] and enhanced by Scheiba [10]. Small slices of the MEA were cut off and embedded in epoxy resin in order to stabilize the electrode's structure. After an additional step of trimming the embedded MEA slices with a razor knife, the samples were microtomed and thin sections with thicknesses between 30 and 500 nm were cut off the MEA. This sample preparation technique allows characterizing MEA samples without having to deal with pore damage or agglomerate pull-out. In addition to the presented electron microscopy methods, Hg porosimetry can be performed in order to obtain porosity, pore size distribution and tortuosity of a porous material [11]. 3D properties, such as pore elongation or information on the so-called open porosity, however, cannot be determined by any of these techniques, neither by electron microscopy, nor by Hg porosimetry. Consequently, a method has to be found, which allows for 3D characterization of the electrode structure.

In 2001 Inkson et al. [12] published the 3D characterization of a metallic nanocomposite by Focused Ion Beam (FIB) tomography. Starting from there, FIB tomography was developed further and found application in several fields of interest such as biology [13], metallurgy [14, 15], and medicine [16]. Wilson et al. [17] were able to reconstruct a defined volume of a solid oxide fuel cell (SOFC) anode with the three different phases Ni, yttrium-stabilized zirconia (YSZ) and pore space. The obtained data allowed them to build a 3D map of the TPB in the anode and its state of connection to the microstructure. They were able to show that about 60% of the TPB is linked to the rest of the microstructure, whereas about 20% of the TPB consists of short length and are not connected to the rest of the microstructure at all. The remaining fraction of the TPB is connected to parts of the microstructure, but its overall connection was hard to characterize due to the small reconstructed volume.

First results in 3D reconstruction concerning PEMFCs were published by Ostadi et al. [18]. They analyzed a hydrophobic carbon-based microporous layer (MPL) for PEMFCs using FIB tomography with respect to porosity and pore size distribution. A lattice Boltzmann numerical solver was used to simulate a single-phase flow through the MPL enabling the calculation of permeability and tortuosity of the layer.

State-of-the-art FIB instrumentation enabled us to perform FIB sectioning on PEMFC electrodes. The electrodes are highly porous and due to their structure in general very sensitive to sample damage and imaging artifacts. In this work, two differently prepared MEAs were sectioned by FIB and the reconstructed volumes were analyzed regarding porosity, pore size and tortuosity. Beyond that, ultramicrotomic thin-sections were characterized by SEM with respect to porosity. Polarization curves of the MEAs were recorded in order to point out the structural influence on the PEMFC performance.

## 2 Experimental

### 2.1 Membrane electrode assembly preparation

In this study, MEAs were manufactured using two different fabrication processes. A reference MEA was prepared by a slightly modified airbrushing method (hereinafter referred to as AB), which was first published by Wilson et al. [19] For the second MEA (multilayered MEA, hereinafter referred to as ML) a novel fast spraying technique [20] was used, which is based on the layer-by-layer method [21]. In both cases, 200 mg of commercially available carbon supported Pt catalyst (20 wt-% Pt on Vulcan XC-72, Johnson Matthey, Pt/CB) was used. For the airbrushing method, 1 ml Nafion<sup>®</sup> solution (5 wt-% in lower aliphatic alcohols and water, Sigma-Aldrich), 2-3 drops of glycerin, 4 ml isopropanol and 12 ml MilliQ water were added and homogenized by ultrasound. The catalyst ink was coated onto both sides of a heated ( $T = 100\text{ }^{\circ}\text{C}$ ) and horizontally mounted Nafion<sup>®</sup> 117 membrane (DuPont<sup>™</sup>, thickness 183  $\mu\text{m}$ ) using an airbrush (Evolution Two in One, Harder & Steenbeck, Germany). After one layer of catalyst ink was sprayed onto the membrane, it was waited until this layer was completely dry. This procedure was repeated, until the catalyst ink was sprayed completely onto the membrane. For the fast spray coating technique two dispersions were prepared. The first dispersion consisted of 200 mg Pt/CB, 10 ml MilliQ, 50 ml isopropanol and 2 drops of glycerin. The second dispersion contained 1 ml Nafion<sup>®</sup> solution dispersed in 50 ml isopropanol. The fast spray coating was performed at 120  $^{\circ}\text{C}$  using ecoSpray<sup>®</sup> spraying containers (Labo Chimie, France). In contrast to the airbrushing method, the Nafion<sup>®</sup> 117 membrane was mounted upright and the two dispersions were sprayed alternately onto the membrane for 4 s, respectively, starting with a layer of Pt/CB catalyst. The higher preparation temperature ensured a fast evaporation of the dispersing agent and prevented drainage of the catalyst material.

## 2.2 Characterization

FIB nanotomography was performed using a Zeiss 1540EsB CrossBeam<sup>®</sup> with an ultra-high resolution GEMINI<sup>®</sup> e-Beam column and a high performance Canion gallium ion column. A Pt protective layer with a thickness of 700 nm was applied to the MEA by the Gas Injection System (GIS) in order to minimize the redeposition effect. A FIB serial sectioning and SEM imaging sequence based on the work of Holzer et al. [22] was used for obtaining slices of nominally 12.5 nm (AB MEA) and 14.5 nm (ML MEA) thickness. FIB ion milling, using a 30 kV Ga<sup>+</sup> ion beam with beam currents of 200 pA (AB MEA) and 100 pA (ML MEA), respectively, was carried out. The SEM was operated at an acceleration voltage of 2 kV and with a high efficiency annular type in-lens secondary electron (SE) detector providing nanoscale topographic information. For the AB MEA, 192 FIB slices have been prepared, with a milling time of 10 s and an image processing time of 20.2 s per SE image. 108 FIB slices with a milling time of 15 s have been prepared for the ML MEA. The image processing step after each milling step took 20.2 s.

Alignment of the image stacks was obtained via a recursive method using a fiducial mark and the software ImageJ with StackReg Plugin [23]. A representative subvolume was defined and binarized using the Otsu thresholding algorithm [24]. The Otsu thresholding algorithm works as follows: Every possible threshold for the image is calculated and the pixels are divided into object and background pixels. The spread of the pixel levels on each side of the threshold is calculated and the optimal threshold is found by minimizing the sum of the object and background pixel spreads. This algorithm was applied using the software MAVI (modular algorithms for volume images, Fraunhofer ITWM; Kaiserslautern, Germany). For the 3D visualization of the 2D binarized image datasets, the commercial visualization software package VGStudioMax 2.0 was employed. The voxel size of the reconstructed AB MEA (9.3 nm × 9.3 nm × 12.5 nm) and the voxel size of the ML MEA (14.8 nm × 14.8 nm × 14.5 nm) differ due to adjustments of the FIB software.

The reconstructed 3D volumes provide information about the samples' porosity, pore size distribution and tortuosity. This information was obtained with the software packages VGStudioMax 2.0, LINCE [25], and MAVI. Therefore, pore spaces have been considered as connected spheres.

Ultramicrotomic thin-sections of the MEAs with thicknesses of 200 nm were prepared as described by Scheiba [10]. The thin-sections were investigated using a FEI Quanta 200 FEG SEM equipped with a field emission gun, operating at an acceleration voltage of 15 kV. In addition to the FIB investigations, the semi-automatic software LINCE was used to analyze the SE micrographs of the thin-sections with respect to porosity, pore size distribution and electrode thicknesses. A minimum of ten SEM micrographs was analyzed for every MEA. Standard deviations were calculated for the mean pore sizes and electrode thicknesses of both MEAs.

Determination of the MEAs' platinum loading was performed by thermogravimetric analysis (TGA) using a Netzsch STA 449C Jupiter under synthetic air (Linde, 80% N<sub>2</sub>, 20% O<sub>2</sub>) in a range from 30 to 1035 °C with a heating rate of 5 °C min<sup>-1</sup>.

## 2.3 Single cell tests

Fuel cell tests were carried out on fresh MEAs using an in-house built manually operated single cell test bench in hydrogen/oxygen operation. A 25 cm<sup>2</sup> Electrochem. Inc. column flow pattern fuel cell at T<sub>cell</sub> = 80 °C was used. Humidified hydrogen (N 5.0, Linde, T<sub>humidifier</sub> = 75 °C) was fed to the anode with a flow rate of 200 ml min<sup>-1</sup>. The cathode was fed with oxygen (N 3.5, Linde) at a flow rate of 100 ml min<sup>-1</sup>. Polarization curves were recorded galvanostatically after seven days of conditioning at 3 A using an electronic load and a potentiometer.

## 3 Results and discussion

### 3.1 Focused Ion Beam nanotomography

After alignment and reconstruction of the SE images, 3D visualizations of the two MEAs were assembled and are shown in Figures 1a and b. The z-direction represents the FIB milling direction. The grey color in Figure 1 represents the solid phase (carbon supported Pt), the free volume displays the pore phase. The 3D reconstruction of the ML MEA (Figure 1b) features a more homogeneous porosity compared to the reconstructed AB MEA volume (Figure 1a). Furthermore, the AB MEA shows a high number of large, elongated pores and higher agglomeration. The large elongated pores can be explained by the preparation. Since the ink is applied via successive thin layers, the drying process of each layer leads to surface cracks, which are covered with ink in the next airbrushing step. Another preparation effect explains the agglomeration of catalyst in the AB MEA. During the airbrushing process, the catalyst ink is sprayed onto the horizontally mounted membrane and the solid component of the ink sinks down towards the membrane due to a slower evaporation of the dispersing agents. This results in a vertical catalyst gradient in the electrode. For the fast spray coating technique, these effects are prevented by the technique itself and by the modification of the preparation design regarding the membrane mounting. With respect to the porosity, the ML MEA appears to reach higher porosities than the AB MEA. This assumption is confirmed by measurements performed with the software package VGStudioMax 2.0 and further investigations of ultramicrotomic thin sections with SEM.

### 3.2 Scanning electron microscopy analysis on ultramicrotomic thin-sections

SE and backscattered electron (BSE) micrographs of the ultramicrotomed AB and ML MEAs are presented in Figure 2. Although the same amounts of catalyst and ionomer were used in both cases, the novel fast spray coating technique resulted in electrodes with a thickness (Figure 2c,  $d_{ML} = 23.8 \text{ nm} \pm 1.9 \text{ nm}$ ) more than four times larger than those prepared by airbrushing (Figure 2a,  $d_{AB} = 5.5 \text{ nm} \pm 0.7 \text{ nm}$ ) also pointing towards the higher porosity in the former case. With the help of a mathematical model Boyer, et al. [26] stated that the current density of a MEA increases with a smaller electrode thickness. Wang et al. [27] proved this model, and showed that especially in the region of high current densities a thicker electrode acts as a mass diffusion barrier. Furthermore, additional catalyst material compared to thinner electrodes with thereby smaller catalyst amount appears to have no effect on the cell reaction. For the ML MEA, it can be concluded that a lower amount of catalyst per electrode will result in a higher performance and accordingly a higher platinum utilization. This will be the objective of future work.

Comparing both MEAs, the structure of the ML MEA shows a high homogeneity. In addition to the more homogeneous distribution of the pores in the ML MEA, the pore size distribution (Figure 3) is narrower for the ML MEA ( $d_{ML,mean} = 118 \text{ nm} \pm 76 \text{ nm}$ ) than for the AB MEA ( $d_{AB,mean} = 233 \text{ nm} \pm 143 \text{ nm}$ ). This also points to a more homogeneous structure of the ML MEA. **The high standard deviation of the mean pore sizes is due to the broad pore size distributions.** Furthermore, agglomeration of the catalyst particles, as it is visible in the AB MEA (Figure 2b), was hindered by the fast spray coating technique. A homogeneous distribution of the Pt nanoparticles in the electrode of the ML MEA (Figure 2d) was reached. **O'Hayre et al. [28] claim that the electrode structures should be on the order of the size of the TPB width or smaller. According to their assumption, our more homogeneous pore distribution and structure with smaller pore sizes of the ML MEA should thus result in an increased performance despite its larger electrode thickness.**

### 3.3 Porosity, pore size distribution and tortuosity

Based on the 3D reconstruction of the MEAs' microstructure, an analysis of the porosity, pore size distribution and tortuosity of both samples could be processed as a volume analysis. However, supplementary to the FIB microstructure analysis SEM ultramicrotomic thin-sections (Figure 2) were characterized with the semi-automatic software LINCE [25] to validate the structural parameters (Table 1).

The porosimetry measurements performed on both the reconstructed 3D volume and the ultramicrotomic thin-sections show a good agreement of the two corresponding methods. The ML MEA reaches a 15 to 20% higher porosity compared to the AB MEA in both cases. The mean pore size of the ML MEA is half of the AB MEA's mean pore size. In combination with the higher porosity this has a positive effect on the Pt utilization of the ML MEA. A recent study by Zhang et al. [4] demonstrated the positive influence of higher electrode porosity on the water management in PEMFCs. Furthermore, a higher porosity is linked to an increase of the TPB and, therefore, a higher Pt utilization. This was confirmed by the Pt utilization analysis of the two MEAs by TGA measurements. The Pt utilization of the ML MEA is  $1962 \text{ mW mg}^{-1}$ , exceeding the AB MEA's Pt utilization of  $879 \text{ mW mg}^{-1}$  by far. Hence, the 20% higher porosity leads to an increase of the Pt utilization by a factor of nearly 2.5. Beyond that, TGA analysis showed that only 40% of the carbon supported Pt catalyst used for the AB MEA (40.6 mg) was needed for the ML MEA (16.3 mg) to reach the same performance. This represents a cost reduction of 60% for MEA fabrication.

**Contrary to the tortuosity based on flow simulations as calculated by Ostadi [18], the geometric tortuosity is calculated in this work.** The geometric tortuosity  $\tau$  is defined as the quotient of the mean effective length of a pore ( $l_{eff}$ ), and the thickness of the layer ( $l$ ) (Eq. (1)). Similar tortuosities were observed for both samples.

$$\tau = l_{eff} / l \quad (1)$$

The mean tortuosities **in the main gas flow direction (y-direction)** of both MEAs of **1.09 (AB MEA) and 1.11 (ML MEA)** indicate a high number of pores with a nearly direct connection between gas diffusion layer and the Nafion® membrane. A direct connection enhances the gas transport within the electrodes and is favored for the removal of liquid water out of the cell.

### 3.4 Single cell tests

Both fabricated MEAs were tested **as described in section 2.3** in an in-house built single cell test bench using the same testing conditions. Polarization curves were recorded and power density curves were calculated on the basis of the polarization curves (Figure 4). The polarization curves show a higher open circuit voltage for the ML MEA compared to the AB MEA. In contrast, the AB MEA reached slightly higher current densities. With respect to the maximal power densities, the two MEAs reached almost the same values ( $p_{ML,max} = 210 \text{ mW cm}^{-2}$ ,  $p_{AB,max} = 218 \text{ mW cm}^{-2}$ ). Mean maximum power densities were calculated from polarization curve measurements recorded over **five days of operation by summing up the individual values and dividing it by the number of values.** A higher mean maximum power density is obtained for the ML MEA ( $p_{ML,mean} = 189 \text{ mW cm}^{-2} \pm 18 \text{ mW cm}^{-2}$ )

compared to the AB MEA ( $p_{AB,mean} = 179 \text{ mW cm}^{-2} \pm 22 \text{ mW cm}^{-2}$ ). Furthermore, the maximum power densities of the ML MEA decrease less drastically over time. This can be explained by the electrode structure and the improved water management of the ML MEA compared to the AB MEA. The ML MEA may therefore be better suited for long-term applications than the AB MEA. **This has to be further confirmed in future degradation studies.**

## 4 Conclusion

Two MEAs, one airbrushed and one fabricated by the novel layer-by-layer inspired fast spray coating technique, were investigated with respect to their porosity, pore size distribution, tortuosity, Pt utilization and performance. FIB nanotomography, SEM on ultramicrotomic thin-sections, TGA measurements and single cell tests were performed. **To our knowledge, we were the first to apply the FIB nanotomography technique to differently prepared MEAs for PEMFCs, although the suitability of FIB nanotomography as a 3D structure characterization method for PEMFCs has also been demonstrated by Schwanitz et al. [29]. The results obtained by the 3D analysis show good agreement to the 2D SEM analysis. The investigations showed that the ML MEA features a more homogeneous porosity and pore size distribution. The Pt utilization of the ML MEA ( $1962 \text{ mW cm}^{-2}$ ) was more than 2 times higher than the Pt utilization of the AB MEA ( $879 \text{ mW cm}^{-2}$ ). Furthermore, the advantages of the novel spray coating technique are, e.g. a high homogeneity of the electrode with respect to pore size, Pt distribution, and especially the cost reduction of 60% due to the decreased catalyst amount. According to the mathematical models [26, 27], which claim a higher current density and performance for a MEA with a thinner electrode, further investigations on a ML MEA with a decreased electrode thickness will be performed.**

## Acknowledgments

Financial support of the Deutsche Forschungsgemeinschaft (DFG) is gratefully acknowledged. Parts of the project were funded by the German Federal Ministry of Education and Research (BMBF) under Grant No. 03SF0324. The authors thank C. Fasel for the thermogravimetric analysis measurements.

## References

- [1] M. Eikerling, A. A. Kornyshev, *J. Electroanal. Chem.*, **2001**, 502, 1.
- [2] M. Eikerling, S. Paddison, L. Pratt, T. Zawodzinski, *Chem. Phys. Lett.*, **2003**, 368, 108.
- [3] C. Hartnig, I. Manke, R. Kuhn, N. Kardjilov, J. Banhart, W. Lehnert, *Appl. Phys. Lett.*, **2008**, 92, 134106.
- [4] F. Y. Zhang, D. Spornjak, A. K. Prasad, S. G. Advani, *J. Electrochem. Soc.*, **2007**, 154, B1152.
- [5] D. R. Rolison, *Science*, **2003**, 299, 1698.
- [6] M. Luo, C. Huang, W. Liu, Z. Luo, M. Pan, *Int. J. Hydrogen Energy*, **2010**, 35, 2986.
- [7] M. Schulze, M. von Bradke, R. Reissner, M. Lorenz, E. Gulzow, *Fresenius' J. Anal. Chem.*, **1999**, 365, 123.
- [8] J. Xie, F. Garzon, F. Zawodzinski, W. Smith, *J. Electrochem. Soc.*, **2004**, 151, A1084.
- [9] D. A. Blom, J. R. Dunlap, T. A. Nolan, L. F. Allard, *J. Electrochem. Soc.*, **2003**, 150, A414.
- [10] F. Scheiba, Ph.D. Thesis, Technische Universität Darmstadt, Darmstadt, Germany, **2008**.
- [11] J. Lobato, P. Canizares, M. A. Rodrigo, J. J. Linares, D. Ubeda, F. J. Pinar, *Fuel Cells*, **2010**, 10, 312.
- [12] B. J. Inkson, M. Mulvihill, G. Mobus, *Scr. Mater.*, **2001**, 45, 753.
- [13] D. A. M. De Winter, C. T. W. M. Schneijdenberg, M. N. Lebbink, B. Lich, A. J. Verkleij, M. R. Drury, B. M. Humbel, *J. Microsc. (Oxf.)*, **2009**, 233, 372.
- [14] F. Lasagni, A. Lasagni, M. Engstler, H. P. Degischer, F. Mücklich, *Adv. Eng. Mater.*, **2008**, 10, 62.
- [15] A. J., Kubis, G. J. Shiflet, D. N. Dunn, R. Hull, *Metall. Mater. Trans. A*, **2004**, 35A, 1935.
- [16] L. H. P. Hekking, M. N. Lebbink, D. A. M. De Winter, C. T. W. M. Schneijdenberg, C. M. Brand, B. M. Humbel, A. J. Verkleij, J. A. Post, *J. Microsc. (Oxf.)*, **2009**, 235, 336.
- [17] J. R. Wilson, W. Kobsiriphat, R. Mendoza, H. Y. Chen, J. M. Hiller, D. J. Miller, K. Thornton, P. W. Voorhees, S. B. Adler, S. A. Barnett, *Nat. Mater.*, **2006**, 5, 541.
- [18] H. Ostadi, P. Rama, Y. Liu, R. Chen, X. X. Zhang, K. Jiang, *J. Membr. Sci.*, **2010**, 351, 69.
- [19] M. S. Wilson, S. Gottesfeld, *J. Electrochem. Soc.*, **1992**, 139, L28.
- [20] A. Wolz, S. Zils, M. Michel, C. Roth, *J. Power Sources*, **2010**, DOI: 10.1016/j.jpowsour.2010.06.087.
- [21] G. Decher, *Science*, **1997**, 277, 1232
- [22] L. Holzer, F. Indutnyi, P. H. Gasser, B. Munch, M. Wegmann, *J. Microsc. (Oxf.)*, **2004**, 216, 84.
- [23] P. Thevenaz, U. E. Ruttimann, M. Unser, *IEEE Trans. Image Process.*, **1998**, 7, 27.
- [24] N. Otsu, *IEEE Trans. Sys. Man. Cyber.*, **1979**, 9, 62.
- [25] S. L. dos Santos e Lucato, Lince v 2.31. TU Darmstadt, FB Materials Science, Ceramics Group, **1999**.
- [26] C. C. Boyer, R. G. Anthony, A. J. Appleby, *J. Appl. Electrochem.*, **2000**, 30, 777.
- [27] Q. Wang, D. Song, T. Navessin, S. Holdcroft, Z. Liu, *Electrochim. Acta*, **2004**, 50, 725.
- [28] R. O'Hayre, D. M. Barnett, F. B. Prinz, *J. Electrochem. Soc.*, **2005**, 152, A439.

[29] B. Schwanitz, H. Schulenburg, J. Krbanjevic, M. Stampanoni, A. Wokaun, G. G. Scherer, *Book of Abstracts: International Symposium TRANSPORE 2010*, 2010, 84.

## Figure Captions

Figure 1 3D visualization of a) the AB MEA and b) the ML MEA prepared by FIB nanotomography.

Figure 2 a) SE and b) BSE micrograph of the AB MEA; c) SE and d) BSE micrograph of the ML MEA.

Figure 3 Pore size distribution of the AB (black columns) and ML (grey columns) electrodes. Log Normal fits are displayed in black solid (AB) and black dashed (ML) lines.

Figure 4 Polarization and power density curves of the a) AB MEA and the b) ML MEA.

## Tables

Table 1 Pore parameters from imaging. The porosity by FIB nanotomography was obtained via a thresholding method. The porosity by ultramicrotomic thin-section as well as the mean pore sizes by FIB nanotomography and ultramicrotomic thin-sections were obtained via the semi-automatic software LINCSE. Determination of the mean geometric tortuosity was performed by via digital path measurements of the reconstructed sample volumes.

	AB	ML
<b>Porosity by FIB nanotomography</b>	44.9% ± 5.0%	62.6% ± 5.0%
<b>Porosity by ultramicrotomic thin-section</b>	37.3% ± 5.0%	56.4% ± 5.0%
<b>Mean pore size by FIB nanotomography</b>	233 nm ± 143 nm	118 nm ± 76 nm
<b>Mean pore size by ultramicrotomic thin-sections</b>	334 nm ± 47 nm	113 nm ± 143 nm
<b>Mean geometric tortuosity in y-direction</b>	1.09 ± 0.06	1.11 ± 0.06

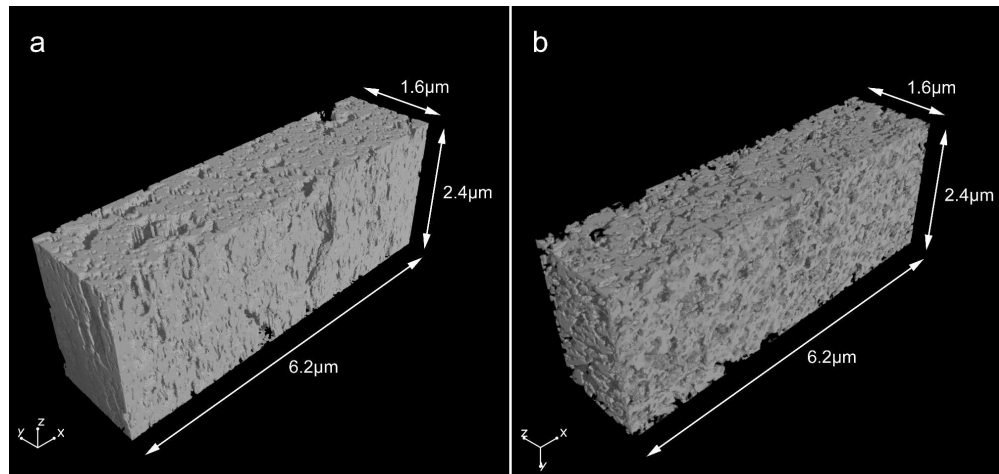


Figure 1 3D visualization of a) the AB MEA and b) the ML MEA prepared by FIB nanotomography.  
170x80mm (600 x 600 DPI)

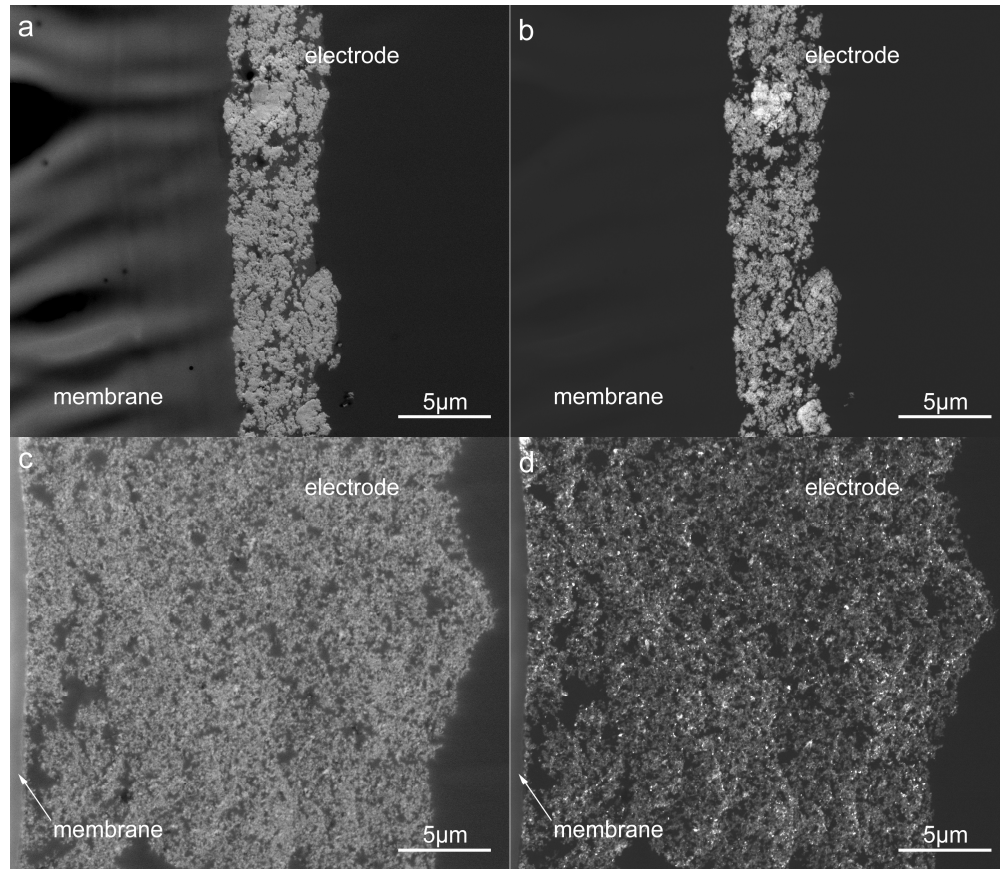


Figure 2 a) SE and b) BSE micrograph of the AB MEA; c) SE and d) BSE micrograph of the ML MEA.  
139x120mm (600 x 600 DPI)

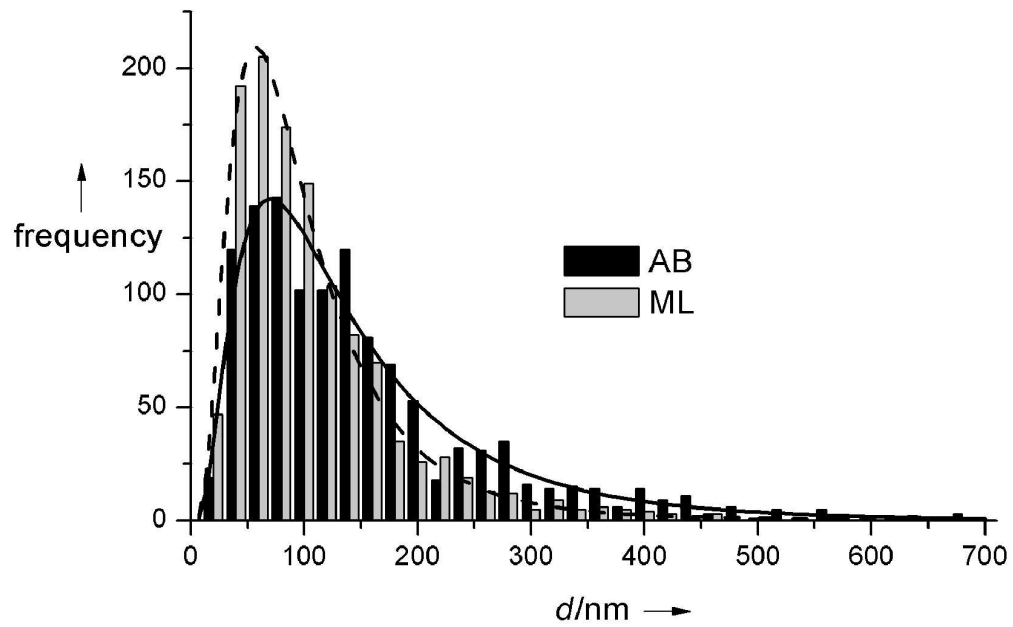


Figure 3 Pore size distribution of the AB (black columns) and ML (grey columns) electrodes. Log Normal fits are displayed in black solid (AB) and black dashed (ML) lines.  
70x43mm (600 x 600 DPI)

1  
2  
3  
4  
5  
6  
7  
8  
9  
10  
11  
12  
13  
14  
15  
16  
17  
18  
19  
20  
21  
22  
23  
24  
25  
26  
27  
28  
29  
30  
31  
32  
33  
34  
35  
36  
37  
38  
39  
40  
41  
42  
43  
44  
45  
46  
47  
48  
49  
50  
51  
52  
53  
54  
55  
56  
57  
58  
59  
60

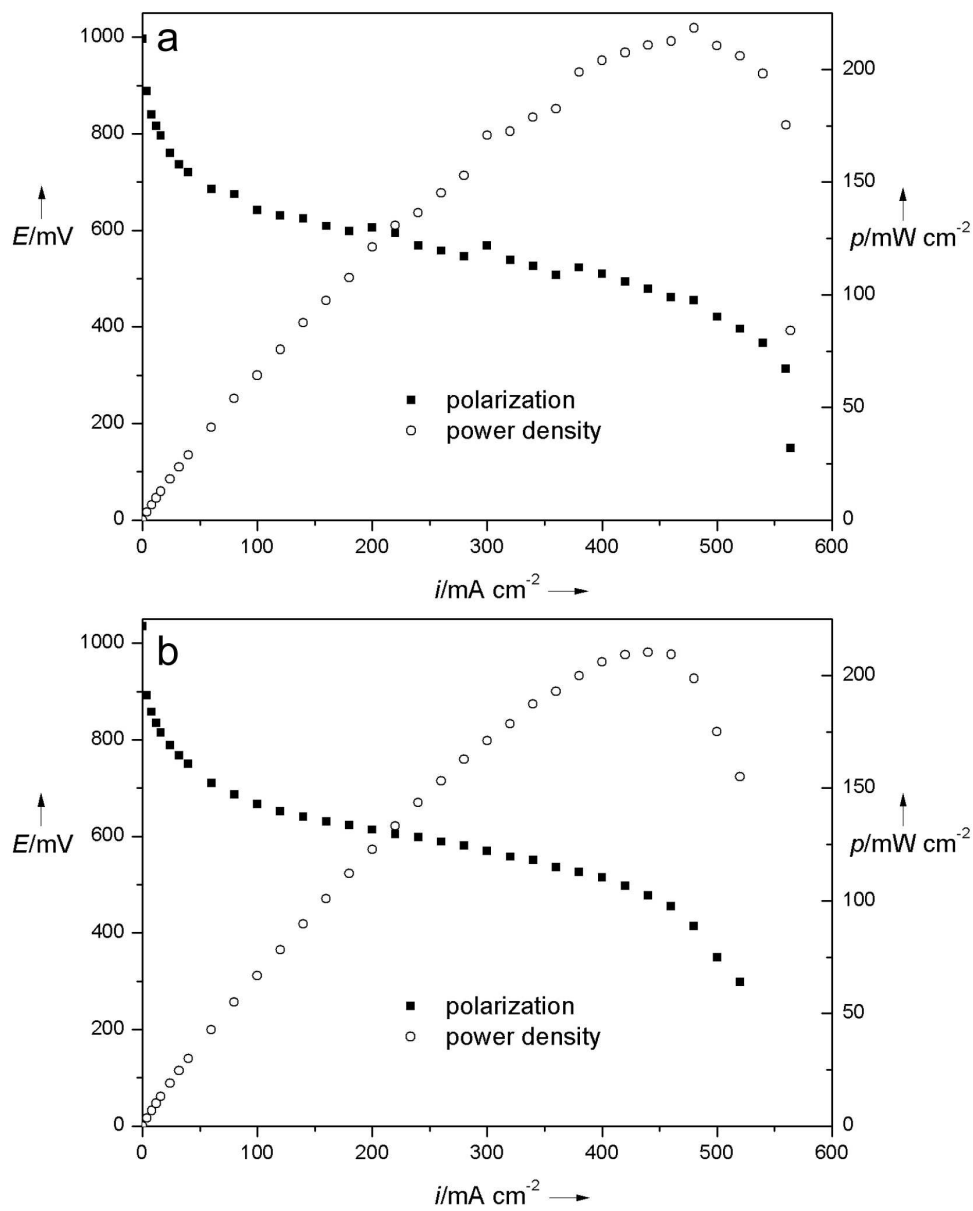


Figure 4 Polarization and power density curves of the a) AB MEA and the b) ML MEA. 70x87mm (600 x 600 DPI)